applied sciences

MDPI

Article

Study on Dynamic Mechanical Properties and Failure Pattern of Thin-Layered Schist

Yaxiong Peng [1,2,3,*], Zehui Du [4], Peng Chen [3], Yingkang Yao [1,2,*], Guangjin Liu [5] and Li Wu [5]

[1] State Key Laboratory of Precision Blasting, Jianghan University, Wuhan 430056, China
[2] Hubei Key Laboratory of Blasting Engineering, Jianghan University, Wuhan 430056, China
[3] Hunan Provincial Key Laboratory of Geotechnical Engineering for Stability Control and Health Monitoring, School of Civil Engineering, Hunan University of Science and Technology, Xiangtan 411201, China; 16673100967@163.com
[4] Hubei Key Laboratory of Advanced Materials & Reinforcement Technology Research for Marine Environment Structures, CCCC Wuhan Harbour Engineering Design and Research Co., Ltd., Wuhan 430040, China; 18627905108@163.com
[5] Engineering Research Center of Rock-Soil Drilling & Excavation and Protection, Ministry of Education, China University of Geosciences, Wuhan 430074, China; liuguangjin1997@163.com (G.L.); lwu@cug.edu.cn (L.W.)
* Correspondence: 1020172@hnust.edu.cn (Y.P.); shanxiyao@jhun.edu.cn (Y.Y.)

Abstract: This paper studies the effect of schistosity on the dynamic mechanical properties and failure pattern of thin-layered schist. Wudang Group schist with thin layers is selected as the research object, and the influence of the dynamic mechanical properties and failure pattern of schist under different angles and spacing is studied by combining an SHPB test and numerical simulation. The results indicate that under dynamic loading, the stress–strain curve demonstrates elastic compression, plastic deformation, and strain softening stages. Moreover, it is observed that the dynamic critical failure strength of schist exhibits typical "U"-type strength anisotropy. Specimens with a schistosity angle of 0° or 90° exhibit higher dynamic compressive strength under dynamic loading, with axial splitting and schistosity splitting as predominant failure modes. Conversely, when the schistosity angles are 30°, 45° or 60°, there is a noticeable decrease in compressive strength accompanied predominantly by shear failure along with local compressive shear failure. We additionally noted that as the spacing between schists decreases from 22 mm to 7 mm, there is a gradual reduction in dynamic compressive strength by approximately 20.3%.

Keywords: thin-layered schist; schistosity; dynamic mechanical properties; SHPB

check for updates

Citation: Peng, Y.; Du, Z.; Chen, P.; Yao, Y.; Liu, G.; Wu, L. Study on Dynamic Mechanical Properties and Failure Pattern of Thin-Layered Schist. *Appl. Sci.* **2024**, *14*, 9101. https://doi.org/10.3390/app14199101

Academic Editor: Cheng-Yu Ku

Received: 30 August 2024
Revised: 2 October 2024
Accepted: 7 October 2024
Published: 8 October 2024

Copyright: © 2024 by the authors. Licensee MDPI, Basel, Switzerland. This article is an open access article distributed under the terms and conditions of the Creative Commons Attribution (CC BY) license (https://creativecommons.org/licenses/by/4.0/).

1. Introduction

Stratified rock mass is a discontinuous medium with widespread distribution, characterized by macroscopic bedding. It can be classified into two primary types: metamorphic rocks (such as slate, phyllite, and schist) and sedimentary rocks (including shale, sandstone, and limestone) [1–3]. The mechanical characteristics of layered rock mass are relatively consistent parallel to the layer, while the mechanical properties perpendicular to the layer show significant differences. Due to the anisotropy of stratified rock mass, the failure mode and strength of rock mass in different directions will be different. Therefore, it is very important to master the mechanical properties, failure pattern and stratification effect for stratified rock mass [4,5].

Numerous scholars have conducted research on the intricate mechanical properties of stratified rock mass. For example, Kou et al. [6] investigated the macro and micro fracture behavior of laminated gneiss and discussed the influence of temperature and bedding angle on the tensile strength. Mo et al. [7] revealed that acid treatment affects the failure pattern of layered limestone and found that there are three main failure modes with the change in bedding angle, namely split failure, sliding failure and mixed failure. Shi et al. [8]

explored the relationship between the fracture toughness and tensile strength of shale in relation to the bedding angle and anisotropy degree. Nezhad et al. [9] conducted Brazil splitting tests and finite element simulations on shale to study how bedding and matrix influence tensile strength and fracture toughness. Tien et al. [10] examined the mechanical properties of stratified rock mass along with four typical failure modes using simulated materials. Li et al. [11] utilized uniaxial and triaxial test methods to explore different coal samples' mechanical properties at varying bedding angles.

The previous studies have primarily focused on the mechanical characteristics of layered rock formations under quasi-static loading conditions. However, during tunnel excavation and mining operations, these rock formations are predominantly subjected to dynamic loads. Therefore, it is essential to investigate the dynamic mechanical properties and failure pattern of stratified rock masses under impact loads [12]. Numerous scholars have made significant progress in exploring the dynamic mechanical features of stratified rock formations. Zhao et al. [13] studied the dynamic tensile strength of coal samples under saturated and dry water content conditions using Brazilian disk tension tests. Feng et al. [14] put forward the energy dissipation parameter as an evaluation indicator to study the mechanical characteristics and deformation laws of rock under impact loads. Fan et al. [15] examined the variations in mechanical parameters and failure modes of shale with different bedding angles at varying temperatures. Gong et al. [4] investigated the dissipation of energy during the dynamic fracturing of layered coal rocks. Liu et al. [16] utilized SHPB systems to comprehensively study the dynamic mechanics and absorbed energy of phyllite. Luo et al. [17] performed dynamic triaxial SHPB tests on shales with different bedding angles by numerical simulation and revealed the stress–strain curve, failure process and morphological characteristics of layered shale.

Schist is a metamorphic rock with a typical lamellar structure resulting from regional metamorphism. It is characterized by its schistosity structure, consisting of lamellar, plate-like, and fibrous minerals arranged parallel to each other with a visible grain size. Due to its internal weak schistosity plane, schist is generally considered a transversely isotropic material [18,19]. Xu et al. [20] conducted triaxial compression creep tests to explore the impacts of the foliation direction and stress level on mica schist's creep behavior. Yin et al. [21] revealed anisotropy in wave velocity and peak strength for quartz mica schist, as well as the mechanism for macro-anisotropy. Zuo et al. [22] developed a nonlinear viscoelastic–plastic creep constitutive model, considering the rheological mechanical characteristics, to describe the entire creep process of schist. Zhou et al. [23] carried out triaxial impact tests on dry and saturated schist using improved triaxial split Hopkinson pressure bar system equipment to analyze the coupling effects of the strain rate, water content, and triaxial confining pressure on mechanical properties. Mehmet et al. [24] studied the effect of schist anisotropy on elastic parameters such as dynamic Young's modulus and dynamic Poisson's ratio and discussed the negative effects of water on the dynamic mechanical properties of schist.

As mentioned in previous reviews, there has been limited research on the dynamic properties and effects of schistosity under impact loads for shists. Here, we study Wudang Group schist in the northwestern Hubei region of China, which is a typical thin-layered schist. The dynamic and static properties of thin-layered schist are greatly influenced by the schistosity angle and schistosity spacing. Therefore, this paper focuses on conducting dynamic impact tests using an SHPB test device on thin-layered shists with different angles of schistosity (0°, 30°, 45°, 60°, 90°) to analyze their dynamic mechanical characteristics. And numerical simulations are used to study the effect of angle and thickness on the dynamic mechanical characteristics and failure patterns.

2. SHPB Test

2.1. Specimen Preparation

Wudang Group schist in a high-speed tunnel in northwest Hubei of China is selected as the research object. The schist is thin-layered, gray and uniform in texture. The main mineral composition is mica (63%), dolomite (4%), and quartz (21%), mixed with a small

amount of albite and chlorite. In order to ensure the uniformity of the schist specimen, all specimens are taken from a single intact schist. At the same time, to analyze the influence of schistosity on its dynamic mechanical behavior, 5 groups of different schistosity angles (0°, 30°, 45°, 60° and 90°) are selected for core sampling, and standard cylinder specimens (diameter 50 mm, height 25 mm) with a height to diameter ratio of 0.5 are made, with 3 specimens in each group. The schistosity angle θ is defined as the angle between the schistosity distribution direction and the longitudinal axis of the cylindrical specimen (the loading direction). The specimens are shown in Figures 1 and 2.

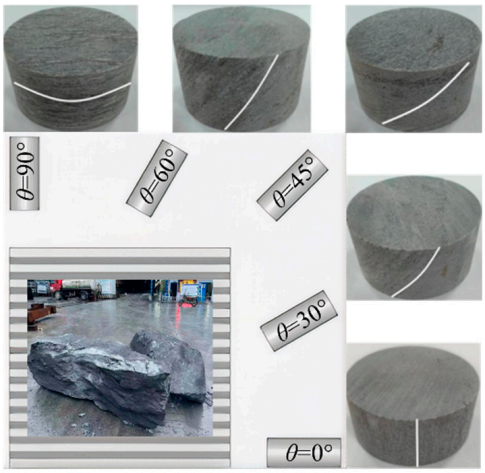


Figure 1. Thin-layered schist with different schistosity angles.

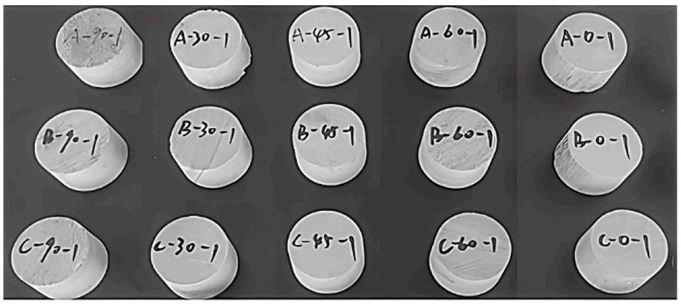


Figure 2. Thin-layered schist specimens in SHPB test.

2.2. Test Equipment

The dynamic compression test employs the split Hopkinson pressure bar system (SHPB), comprising a bullet, incident bar, transmission bar, absorption bar, and data acquisition and recording system. All rods (incident rod, transmission rod, and absorption rod) have a diameter of 50 mm. The incident rod measures 2 m in length while the transmission rod is 1.5 m. Specimens are vertically positioned between the incident and transmission rods with strain gauges attached to each. These strain gauges are linked to a super-dynamic strain gauge and oscilloscope system. During impact, the wave signal from the strain gauge located between the incident and transmission rods is transmitted to the oscilloscope for analysis. Subsequently, computer analysis software processes this waveform diagram to calculate the corresponding loading pulse curve. The schematic diagram of SHPB devices is depicted as Figure 3.

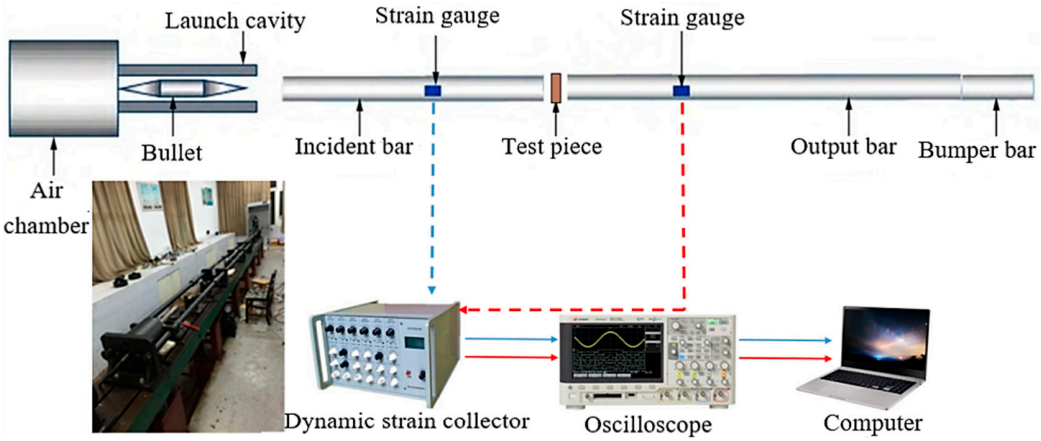


Figure 3. The schematic diagram of SHPB system.

The dynamic compression test was carried out at a constant 0.4 MPa impact pressure. In order to ensure the accuracy of the obtained test results and reduce the data dispersion, three independent specimens were prepared for each schistosity angle; that is, three repeated tests were carried out under each working condition to improve the reliability and stability of the results.

3. Dynamic Mechanical Properties

3.1. Stress Balance

The strain gauges on both the incident rod and the transmission rod are used to measure the incident wave. In Figure 4, a typical stress waveform diagram of a thin-layered schist SHPB test is depicted, and the stress waveforms of each specimen are basically similar. The superimposed curve is generated by overlaying the values of the incident wave and reflected wave at each time, demonstrating that the new curve closely aligns with the transmitted wave. This observation suggests that during the loading process, the schist sample achieved stress equilibrium, thereby indicating the reliability of the test results [25].

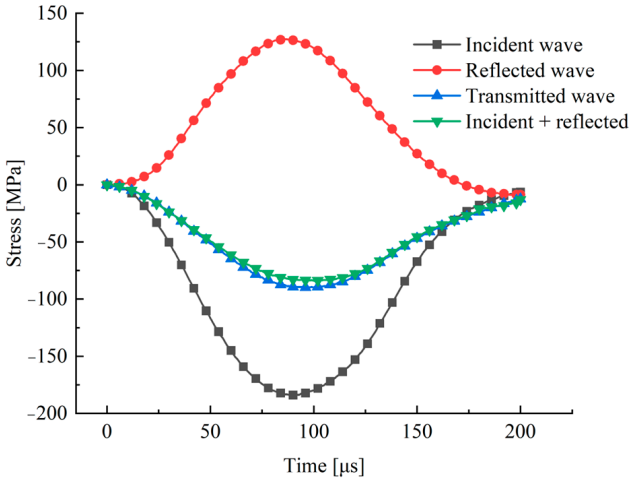


Figure 4. Typical stress wave diagram of thin-layered schist.

3.2. Characteristics of Stress–Strain and Dynamic Strength

The "three-wave method" theory can be used to process the test data and calculate the stress and strain values of specimens [26]. The typical stress–strain curves of each thin-layered schist specimen are obtained by eliminating the obvious abnormal results, as shown in Figure 5.

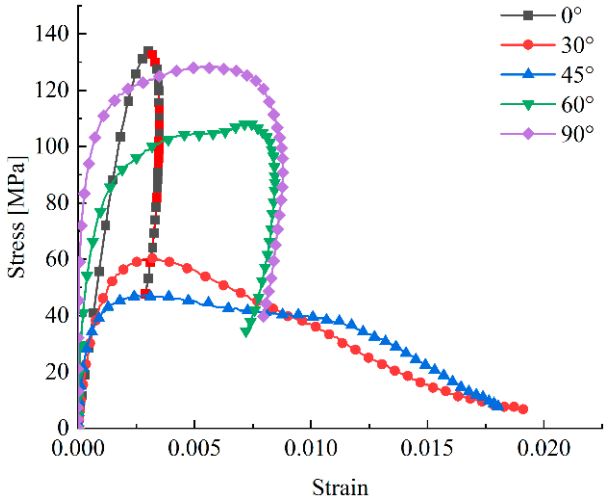


Figure 5. Stress–strain curves of thin-layered schist with different schistosity angles.

According to the stress–strain curve of the specimen, combined with the deformation characteristics of the test, it can be found that the strain process of specimens with different schistosity angles is different, but there are the following stages.

In the first compaction stage, the stress–strain curve shows an obvious downward sag trend; the micro-cracks and pores in the specimen gradually close and shrink under the impact load, and the overall deformation resistance of the specimen is enhanced. Then, the stress–strain relationship of the specimen exhibits linear behavior, that is, linear elastic compression deformation. As deformation progresses, the stress–strain curve gradually becomes concave as the slope decreases and strain increases at a slower rate, and the specimen exhibits plastic deformation.

Since then, variations in curve shapes are observed for thin-layered schist with different schistosity angles. Upon reaching peak stress, there is a rapid decrease in stress with increasing strain, leading to the appearance of a distinct post-peak curve that signifies irreversible deformation damage and failure. The post-peak stress–strain curve of specimens at 0°, 60°and 90° angles has the same downward trend, and the curve is steep, showing a certain brittleness. The curve exhibits closed shapes due to limited fracture without reaching the yield limit, resulting in several large rock blocks. In contrast, the post-peak stress–strain curves of specimens at 30°and 45° angles have a moderate downward trend, which display opening shapes. The rock failure is caused by the shear slip of schistosity.

In addition, the dynamic compressive strength of schist has obvious anisotropy, and different schistosity angles have a significant influence on the overall compressive performance of specimens. When the schistosity angle is 0° and 90°, the specimens show high dynamic compressive strength, and the rock block size after fracture is relatively large. In contrast, specimens with schistosity angles of 30°, 45° and 60° show lower compressive strength values and a higher degree of breakage. The SHPB test results and mean compressive dynamic strength of specimens are shown in Table 1 and Figure 6.

It can be seen from Table 1 and Figure 6 that the dynamic critical failure strength of each thin-layered schist conforms to the typical anisotropy characteristics of "U"-type strength. The compression strength of specimens with schistosity angles of 45° is much lower than in other cases. Combined with the analysis of the failure morphology of the specimens, it can be seen that the specimens with a schistosity angle of 45° fail along the schistosity slip, which is the easiest way to destroy it, so the dynamic compressive strength is the lowest.

Table 1. The SHPB test results.

No.	Schistosity Angle [°]	Volume [cm^3]	Compressive Strength [MPa]			Incident Energy [J]	Reflection Energy [J]	Transmission Energy [J]	Dissipated Energy [J]		
			Value	Mean	Standard Deviation				Value	Mean	Standard Deviation
A-0-1	0	49.04	133.89			74.45	2.99	45.84	25.62		
B-0-1	0	49.08	136.46	136.50	2.63	76.23	3.41	48.15	24.67	25.37	0.61
C-0-1	0	49.10	139.16			74.78	3.67	45.29	25.82		
A-30-1	30	49.07	60.29			72.82	33.84	14.36	24.62		
B-30-1	30	49.10	64.99	60.29	3.14	73.82	36.21	14.56	24.05	24.54	0.450
C-30-1	30	49.03	66.25			72.45	35.67	14.84	24.94		
A-45-1	45	49.06	47.20			67.88	28.81	19.16	19.91		
B-45-1	45	49.04	49.68	49.96	2.90	66.76	29.06	19.34	18.36	18.65	1.13
C-45-1	45	49.11	52.99			68.06	27.56	22.78	17.69		
A-60-1	60	49.06	108.37			84.25	13.67	50.79	19.79		
B-60-1	60	49.13	112.86	111.83	3.07	83.39	14.34	49.45	19.60	19.40	0.51
C-60-1	60	49.09	114.26			86.45	16.16	51.52	18.82		
A-90-1	90	49.06	128.33			98.45	13.78	59.65	25.43		
B-90-1	90	49.10	130.82	130.66	2.26	96.28	13.06	58.43	24.79	24.86	0.54
C-90-1	90	49.02	132.85			96.77	12.98	59.44	24.35		

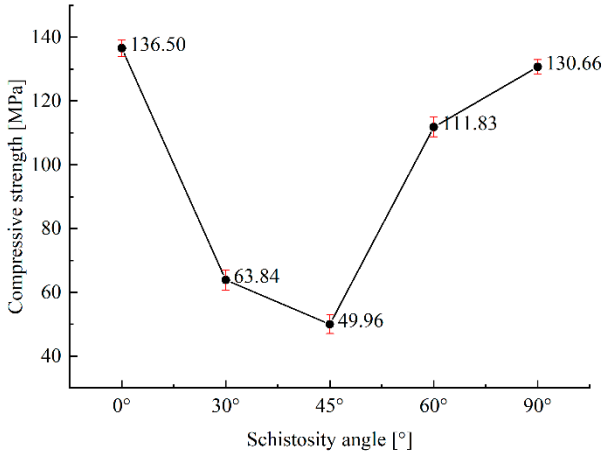


Figure 6. Relationship between the mean dynamic compressive strength and schistosity angle.

3.3. Energy Dissipation Law

According to one-dimensional stress wave theory, the incident energy, the reflection energy and the transmission energy can be calculated by the following formula:

$$\left.\begin{aligned} W_I(t) &= E_0 C_0 A_0 \int_0^\tau \varepsilon_I^2(t)dt \\ W_R(t) &= E_0 C_0 A_0 \int_0^\tau \varepsilon_R^2(t)dt \\ W_T(t) &= E_0 C_0 A_0 \int_0^\tau \varepsilon_T^2(t)dt \end{aligned}\right\} \quad (1)$$

where W_I, W_I and W_T, respectively, are the incident energy, reflection energy and transmission energy. E_0, A_0 and C_0 are the elastic modulus, cross-sectional area and elastic wave velocity of the impact pressure bar, respectively. ε_I, ε_R and ε_T are, respectively, incident, reflected and transmitted strain.

The energy loss between the pressure rod and the rock specimen is ignored during the test and, according to the principle of conservation of energy, can be calculated by the following formula:

$$W_s = W_I - W_R - W_T \quad (2)$$

where W_s is the dissipated energy.

The dissipative energy calculated in Equation (2) includes the total energy absorbed by the sample, the kinetic energy generated by the crushing and flying of the sample, and the heat energy and sound energy in the rock deformation process, amongst others. The

research results show that the latter two kinds of energy account for less than 5% of the total dissipative energy [27]. Therefore, the dissipative energy of the specimen is approximately represented by the total absorbed energy in the SHPB test, which can show how much energy the rock absorbs during the crushing process.

Therefore, according to Equation (2), the incident energy, reflection energy and transmission energy of thin-layered schist specimens at different schistosity angles in the dynamic compression test can be calculated, as shown in Table 1. And the variation law between the schistosity angles and mean dissipated energy are shown in Figure 7.

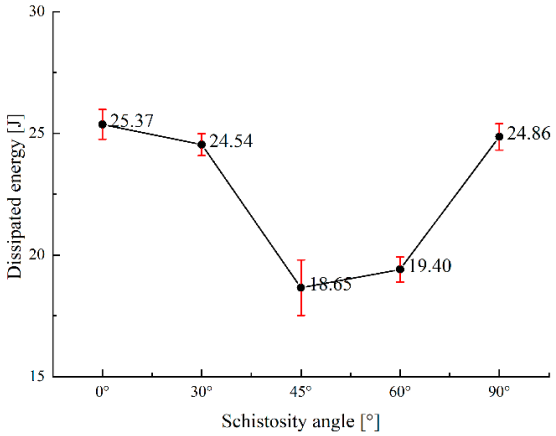


Figure 7. Variation law between the mean dissipated energy and schistosity angle.

As can be seen from Figure 6, the relationship between the dissipated energy and dissipated energy density of the specimen and the schistosity angle presents an approximate "U"-shaped curve feature. The dynamic compressive strength of the specimens with 0° and 90° schistosity angles is the best, which results in the greatest dissipation energy. Although the specimens with 30° schistosity angles are not very strong, more energy is still consumed in the dynamic destruction process. This is because the internal structure of the specimen is broken more violently, resulting in more rock blocks and smaller lumps. Therefore, due to the existence of thin-layered schistosity, the schist failure is characterized by a mixture of splitting, stretching and shearing failure, and its dissipative energy and dynamic compressive strength change law are not completely consistent.

4. Numerical Simulation

4.1. Model and Parameters

Schist is a typical metamorphic rock; the rock mass is relatively broken, and it is difficult to take a relatively complete stone, resulting in a large dispersion of the laboratory test analysis results [28]. In order to further analyze the dynamic mechanical properties and failure pattern of thin-layered schist and discuss the influence of the schistosity angle and schistosity spacing, the SHPB test is numerically simulated using ANSYS/LS-DYNA 18.0.

The simulation model comprises four components corresponding to the actual test system:—the bullet, incident bar, transmission bar, and specimen (Figure 8)—all of which are represented by the three-dimensional solid unit, SOLID164. The model is meshed by the mapping method. The model of the bullet, incident bar, and transmission bar is, respectively, divided into 40, 100 and 80 parts along the radial direction. The specimen model grid was divided into 30 parts to ensure the damage effect of rock mass. The mesh coordination between the incident rod, the transmission rod and the rock specimen can make the simulation results more accurate. A total of 215,400 model units were divided.

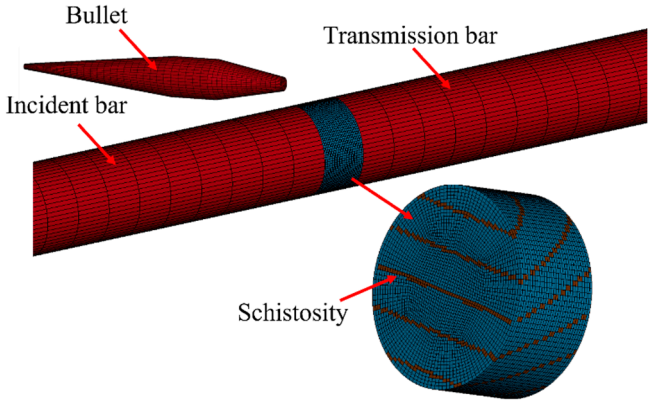


Figure 8. Numerical model of the SHPB system.

AUTOMATIC_NODES_TO_SURFACE is used between the bullet and the incident rod, and ERODING_SURFACE_TO_SURFACE is used between the specimen and the incident rod and transmission rod. The symmetric penalty function algorithm is adopted for the contact surface, and the penalty function factor of the contact stiffness *fs* is 0.8. The unit failure method (MAT_ADD_EROSION) is used to simulate rock sample fracture.

The bullet, incident bar, and transmission bar in the SHPB system are made of 40 Cr alloy steel, which adopts the *MAT_ELASTIC model. The detailed material parameters are ρ = 7900 kg/m^3, E = 210 GPa, and ν = 0.3.

The *MAT_JOHNSON_HOLMQUIST_CONCRETE model is a constitutive model used to simulate the damage and failure of concrete or rock under high load, high strain rate and large deformation [29]. The yield surface equation of the HJC model is described by the dimensionless equivalent stress σ*, and the expression is as follows:

$$\sigma^* = \left[A(1-D) + BP^{*N}\right](1 + C\ln\varepsilon^*) \quad (3)$$

where $\sigma^* = \sigma/f_c$ is normalized equivalent yield strength. σ is equivalent strength. f_c is quasi-static uniaxial compressive strength. A is normalized viscous strength. B is the normalized pressure hardening coefficient. C is the influence coefficient of the strain rate. D is the damage degree. N is the pressure hardening coefficient. P^* is dimensionless pressure, which is the ratio of hydrostatic pressure to compressive strength. ε^* is the dimensionless strain rate.

In this study, this model will be used to study the nonlinear dynamic characteristics of thin-layered schist. According to the SHPB test results of thin-layered schist, specimens with schistosity angles of 90° fracture due to shear failure, and the effect of schistosity is small. Therefore, based on the SHPB laboratory test results, Table 2 displays the HJC parameters of schist.

Table 2. HJC parameters of schist.

ρ	G	A	B	C	N	F_c
2.711	0.068	0.462	1.950	0.240	0.83	4.22×10^{-4}
T	$EPS0$	EF_{min}	S_{max}	P_{crush}	μ_{crush}	P_{lock}
5.31×10^{-5}	1.00×10^{-6}	0.01	5	1.41×10^{-4}	0.00137	0.012
μ_{lock}	D_1	D_2	K_1	K_2	K_3	F_s
0.013	0.04	1	0.279	0.374	0.193	0.5

Due to the unavailability of HJC parameters for the schistosity structure from the SHPB test, we utilized a parameter reduction method to calculate and make a comparison with the test results. Reduction coefficients of 0.4, 0.35, 0.3, 0.25, and 0.2 were employed for comparison purposes. Figure 9 illustrates the comparison between the stress–strain curve obtained through numerical simulation using a reduction coefficient of 0.35 and

dynamic compression test data. The compaction stage and linear elastic stage depicted in the figure demonstrate high consistency between the test data and numerical simulation results. Hence, we determined the reduction coefficient to be 0.35 based on this agreement. However, it is difficult to keep the same angle of each layer plane during the preparation of rock specimens, but numerical simulation can avoid this problem. This leads to unloading stages where the curve differences gradually become apparent.

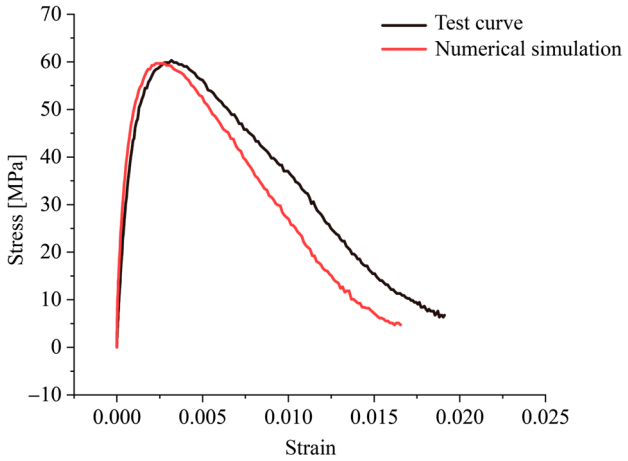


Figure 9. Comparison of stress–strain curves between simulation and experiment.

4.2. Fracture Process

A bullet of impact pressure of 0.4 MPa impacts the schist specimen with a schistosity angle of 30°, and its failure process and von Mises stress are shown in Figure 10. At 399.95 μs, the stress wave from the impacting bar reached the head face of the schist specimen, initiating deformation under impact load. By 469.95 μs, the equivalent stress had peaked and cracks appeared in both the center and periphery of the head face. Around 499.93 μs, damage began to manifest around the end face as facial and lateral cracks became interconnected. Finally, at 579.95 μs, partitioning and spattering of the specimen occurred due to these effects.

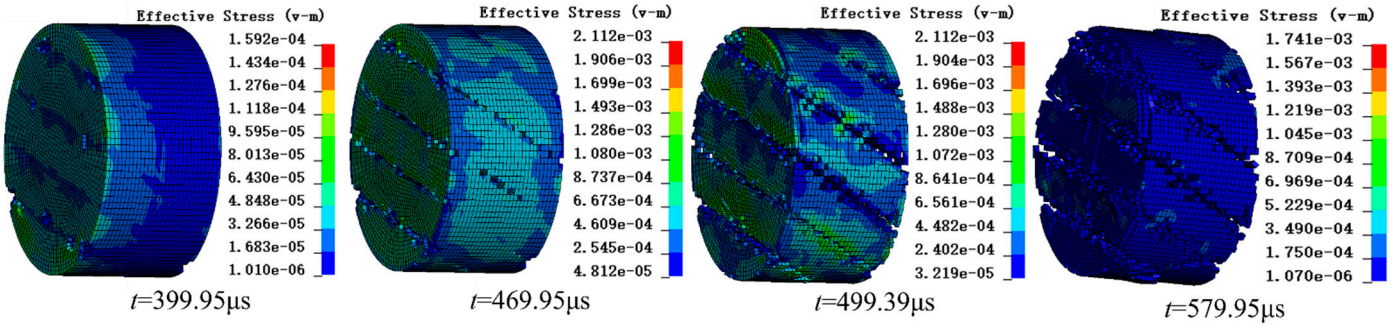


Figure 10. Fracture process simulation.

5. Discussion

5.1. Influence of Schistosity Angle

To further explore the influence of the schistosity angle on the dynamic mechanical properties, numerical models were developed with schistosity angles ranging from 0° to 90° based on the aforementioned model. By integrating laboratory test results and numerical simulations, an analysis was conducted to examine how the schistosity angle impacts the failure pattern of schist, as illustrated in Figure 11. Additionally, the variation in schist dynamic strength with different schistosity angles has been determined through laboratory test analysis.

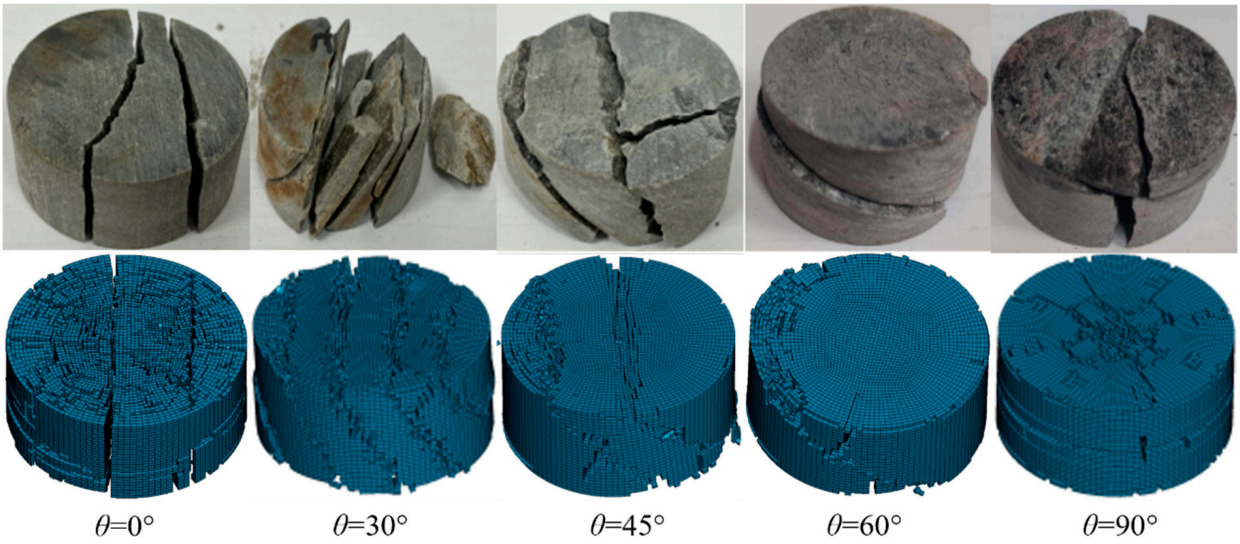


Figure 11. Comparison of failure patterns at different schistosity angles.

It can be seen from Figure 11, it can be clearly seen that the schistosity angle has a significant impact on the failure pattern of thin-layered schist. For specimens with a schistosity angle of 0°, the main failure pattern is axial splitting failure across the schistosity plane, accompanied by local tensile failure along the schistosity plane. This is mainly because under one-dimensional dynamic loading conditions, lateral tensile stress is generated inside the specimen, resulting in cracks developing continuously along the stress wave propagation path from the defect tip, and finally forming axial splitting planes that run through the upper and lower ends of the specimen.

For specimens with schistosity angles of 30°, 45° and 60°, it is observed that the main failure pattern is significant shear failure, accompanied by local compression/shear composite failure characteristics. When the stress wave acts on the directional schistosity, the weak plane of schistosity is subjected to vertical and shear stress parallel to the plane, and the shear fracture along the schistosity plane will be induced. Due to its low shear strength and flexural stiffness perpendicular to the schistosity plane, the compressive shear failure phenomenon of the interpenetrating schistosity plane is displayed in some local areas.

In the specimen with a schistosity angle of 90°, the dynamic compressive failure is mainly manifested as the splitting failure along the schistosity plane. This is because the bonding strength between rock layers is much lower than the strength of the matrix rock itself, so that under the action of lateral tension, axial splitting cracks are first generated at the schistosity.

5.2. Influence of Schistosity Spacing

The schistosity spacing has great influence on the strength of thin-layered schist. It is difficult to collect multiple groups of schist samples with different schistosity spacing within the same or similar areas, which makes it impossible to carry out laboratory rock tests. The above numerical models have verified the feasibility of numerical methods in studying the dynamic characteristics of schist. Therefore, in order to study the influence of schistosity spacing on dynamic mechanical properties, numerical models with schistosity spacing of 22 mm, 17 mm, 12 mm, 9 mm and 7 mm are established. The failure pattern and dynamic compressive strength are, respectively, shown in Figures 12 and 13.

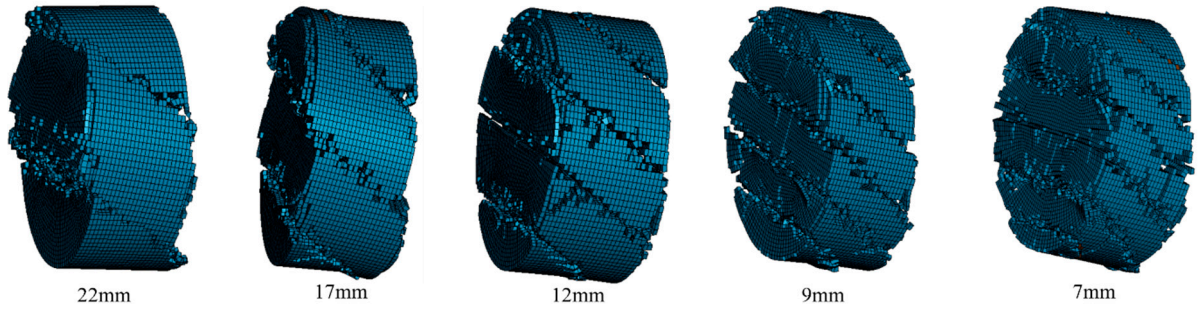


Figure 12. Comparison of failure patterns at different schistosity spacing.

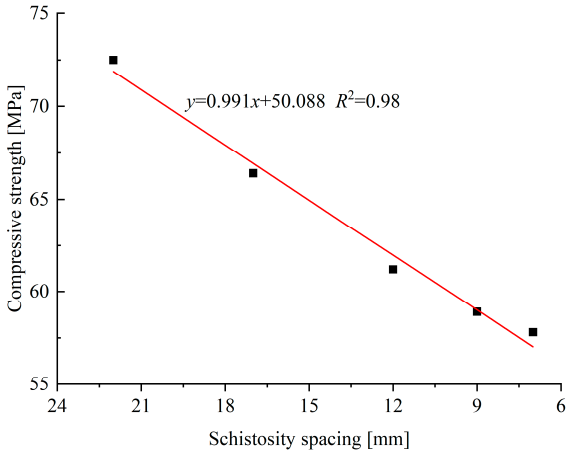


Figure 13. Relationship between the dynamic compressive strength and schistosity spacing.

In Figures 12 and 13, it is observed that the main failure pattern is significant shear failure, and the rock specimens are mainly destroyed along the schistosity under impact load, which indicates that the change in schistosity spacing has little effect on the overall failure pattern. However, with the decrease in schistosity spacing, the damage degree of the rock specimen is higher and more radial cracks are generated along the failure plane of schistosity, which results in a more obvious characteristics accompanied by local compression/shear composite failure. In addition, the dynamic compressive strength decreases gradually with the decrease in schistosity spacing and the change trend is obtained by data fitting. The value drops by up to 20.3% from schistosity spacing of 22 mm to 7 mm.

6. Conclusions

A dynamic impact test (SHPB) is carried out on thin-layered schist with different schistosity angles, the constitutive parameters of rock mass are calibrated by the test results, and the SHPB simulation model is established. The effects of the dynamic mechanical properties and failure pattern of thin-layered schist are studied and the main conclusions of this study are as follows:

(1) The stress–strain curves of thin-layered schist with different schistosity angles are similar, and there are several significant stages in the curve under transient loading, including the elastic compression stage, plastic deformation stage and strain softening stage. The dynamic critical failure strength of each thin-layered schist conforms to the typical anisotropy characteristics of "U"-type strength.

(2) For specimens with schistosity angles of 0°and 90°, the main failure patterns are, respectively, axial splitting failure and splitting failure along the schistosity plane. In the case of thin-layered schists with other schistosity angles, it is observed that the main failure pattern is significant shear failure, accompanied by local compression/shear composite failure characteristics.

(3) With the decrease in schistosity spacing, the main failure pattern of thin-layered schist is significant shear failure; the damage degree of rock specimens is higher and more radial cracks are generated. In addition, the dynamic compressive strength decreases gradually and its value drops by up to 20.3% from the schistosity spacing of 22 mm to 7 mm.

The dynamic mechanical properties and failure pattern of thin-layered schist with different schistosity angles and schistosity spacing are studied. The research results can provide theoretical guidance for schist tunnel blasting excavation and surrounding rock damage prevention and control.

Author Contributions: Methodology, Y.P.; Software, P.C. and Y.Y.; Validation, L.W.; Investigation, Z.D.; Writing—review & editing, G.L. All authors have read and agreed to the published version of the manuscript.

Funding: This research was funded by the State Key Laboratory of Precision Blasting and the Hubei Key Laboratory of Blasting Engineering, Jianghan University (No. PBSKL2022D08); the Scientific Research Project of the Hunan Education Department (Grant no. 22B0486); and the Open Research Foundation of the Engineering Research Center of Rock-Soil Drilling & Excavation and Protection, Ministry of Education (202410). The APC was funded by the State Key Laboratory of Precision Blasting and the Hubei Key Laboratory of Blasting Engineering, Jianghan University, grant number No. PBSKL2022D08.

Institutional Review Board Statement: Not applicable.

Informed Consent Statement: Not applicable.

Data Availability Statement: All data in this article were obtained from the authors' independent experiments and data processing using Origin 2024 software.

Conflicts of Interest: Author Zehui Du was employed by the company CCCC Wuhan Harbour Engineering Design and Research Co., Ltd. The remaining authors declare that the research was conducted in the absence of any commercial or financial relationships that could be construed as a potential conflict of interest.

List of Symbols

Θ	schistosity angle
W_I, W_R and W_T	incident energy, reflection energy and transmission energy
W_s	dissipated energy
E_0, A_0 and C_0	elastic modulus, cross-sectional area and elastic wave velocity of the impact pressure bar
ε_I, ε_R and ε_T	incident, reflected and transmitted strain
ρ	density
E	elastic modulus
N	Poisson's ratio
$\sigma^* = \sigma / f_c$	normalized equivalent yield strength
σ	Equivalent strength
f_c	quasi-static uniaxial compressive strength
A	normalized viscous strength
B	normalized pressure hardening coefficient
C	influence coefficient of strain rate
D	damage degree
N	pressure hardening coefficient
P^*	dimensionless pressure
ε^*	dimensionless strain rate

References

1. Yin, X.; Yan, E.; Wang, L. Anisotropy of quartz mica schist based on quantitative extraction of fabric information. *Bull. Eng. Geol. Environ.* **2020**, *79*, 2439–2456. [CrossRef]

2. Liu, Y.; He, C.; Wang, S.; Peng, Y.; Lei, Y. Dynamic Splitting Tensile Properties and Failure Mechanism of Layered Slate. *Adv. Civ. Eng.* **2020**, *2020*, 1073608. [CrossRef]
3. Zheng, Y.; Zhang, T.; Yang, H.; Wang, W.; Niu, Q.; Wei, H. An Experimental investigation on mechanical properties and failure characteristics of layered rock mass. *Appl. Sci.* **2023**, *13*, 7537. [CrossRef]
4. Shuang, G.; Zhen, W.; Lei, Z. Dynamic fracture mechanics and energy distribution rate response characteristics of coal containing bedding structure. *PLoS ONE* **2021**, *16*, e0247908.
5. Villalobos, F.A.; Rodriguez, P.A.; Vera, M. Study of the anisotropic tensile and compressive strength of a foliated phyllite. *Proc. Inst. Civ. Eng. Geotech. Eng.* **2021**, *176*, 15–26. [CrossRef]
6. Kou, B.; Zhang, D.; Meng, T. Micro and macro evaluation of tensile characteristics of anisotropic rock mass after high temperatures treatment-a case study of Lingshi Gneiss. *Geothermics* **2022**, *102*, 102409. [CrossRef]
7. Mo, Y.; Zuo, S.; Wang, L. Mechanical characteristics of thick-bedded limestone with different bedding angles subjected to acid corrosion. *Bull. Eng. Geol. Environ.* **2022**, *81*, 166. [CrossRef]
8. Shi, X.; Zhao, Y.; Danesh, N. Role of bedding plane in the relationship between Mode-I fracture toughness and tensile strength of shale. *Bull. Eng. Geol. Environ.* **2022**, *81*, 81. [CrossRef]
9. Nezhad, M.; Fisher, Q. Experimental study and numerical modeling of fracture propagation in shale rocks during Brazilian disk test. *Rock. Mech. Rock. Eng.* **2018**, *51*, 1755–1775. [CrossRef]
10. Tien, Y.; Kuo, M. A failure criterion for transversely isotropic rocks. *Int. J. Rock Mech. Min. Sci.* **2001**, *38*, 399–412. [CrossRef]
11. Li, Y.; Zhao, B.; Yang, J.; Sun, J.; Huang, W.; Li, Z.; Wang, B. Experimental study on the influence of confining pressure and bedding angles on mechanical properties in coal. *Minerals* **2022**, *12*, 345. [CrossRef]
12. Qiu, J.; Li, D.; Li, X. Dynamic failure of a phyllite with a low degree of metamorphism under impact Brazilian test. *Int. J. Rock Mech. Min. Sci.* **2017**, *94*, 10–17. [CrossRef]
13. Zhao, Y.; Liu, S.; Jiang, Y.; Wang, K.; Huang, Y. Dynamic tensile strength of coal under dry and saturated conditions. *Rock Mech. Rock Eng.* **2015**, *49*, 1709–1720. [CrossRef]
14. Feng, J.; Wang, E.; Chen, X.; Ding, H. Energy dissipation rate: An indicator of coal deformation and failure under static and dynamic compressive loads. *Int. J. Min. Sci. Technol.* **2018**, *28*, 397–406. [CrossRef]
15. Fan, X.; Luo, N.; Liang, H.; Sun, X.; Zhai, C.; Xie, L. Dynamic Breakage Characteristics of Shale with Different Bedding Angles under the Different Ambient Temperatures. *Rock Mech. Rock Eng.* **2021**, *54*, 3245–3261. [CrossRef]
16. Liu, G.; Peng, Y.; Zuo, Q.; Su, Y.; Wu, L. Dynamic mechanics and energy dissipation of saturated layered phyllite. *Minerals* **2022**, *12*, 1246. [CrossRef]
17. Luo, N.; Zhang, H.; Chai, Y.; Li, P.; Zhai, C.; Zhou, J.; Ma, T. Research on damage failure mechanism and dynamic mechanical behavior of layered shale with different angles under confining pressure. *Deep Undergr. Sci. Eng.* **2023**, *2*, 337–345. [CrossRef]
18. Calmels, F.; Coutard, J. Laboratory experiment on Frost creep mobilization of a heterometric schistous slope. Permafrost. *Periglac.* **2000**, *11*, 207–218. [CrossRef]
19. Zuo, Y.; Han, L.; Hu, H.; Luo, S.; Zhang, Y.; Chen, X. Visco-elastic–Plastic Creep Constitutive Relation of Tunnels. *Soft Schist. Geotech. Geol. Eng.* **2018**, *36*, 389–400. [CrossRef]
20. Xu, J.; Chen, J.; Jiang, P. Investigation of creep behaviors of wudang mica schist by triaxial compression tests. *Geotech. Geol. Eng.* **2019**, *37*, 3831–3842. [CrossRef]
21. Yin, X.; Xia, Z.; Lei, Y. Effect of loading direction on the critical characteristic strength and energy evolution of quartz mica schist and microscale mechanisms. *Bull. Eng. Geol. Environ.* **2021**, *80*, 8693–8710. [CrossRef]
22. Zuo, J.; Wu, L.; Zuo, J.; Lu, L. Study on the constitutive model of visco-elasticity-plasticity considering the rheology of rock mass. *Adv. Mater. Res.* **2013**, *2195*, 567–572.
23. Zhou, Y.; Su, S.; Chen, J. Dynamic response characteristics of dry and water-saturated schist under impact loading. *J. Mt. Sci.* **2020**, *17*, 3123–3136. [CrossRef]
24. Mehmet, Ö.; Sunay, B.; Kaan, E. The effect of anisotropy on the dynamic properties of schist rocks. *J. Sci. Rep. A* **2022**, *49*, 92–104.
25. Liu, S.; Xu, J. Experimental and numerical analysis of Qinling mountain engineered rocks during pulse-shaped SHPB test. *Int. J. Nonlinear Sci. Numer. Simul.* **2015**, *16*, 165–171. [CrossRef]
26. Feng, P.; Liu, B.; Tang, R.; Wei, M.; Zhang, Y.; Li, H. Dynamic fracture behaviors and fragment characteristics of pre-compressed flawed sandstones. *Int. J. Mech. Sci.* **2022**, *220*, 107162. [CrossRef]
27. Ping, Q.; Ma, Q.; Yuan, P. Energy dissipation analysis of stone specimens in SHPB tensile test. *J. Min. Saf. Eng.* **2013**, *30*, 401.
28. Wang, J.; Wang, S.; Chen, Z.; Zou, Y.; Cao, W.; Zhou, J.; Li, C. Influence of inclined joint on dynamic response of rectangular opening subject to blast-induced stress wave. *Arab. J. Sci. Eng.* **2024**. [CrossRef]
29. Fan, Y.; Chen, J.; Leng, Z.; Yang, G.; Liu, X.; Tian, B. Punching mechanism of air-deck stemming for drilling blasting and its influence on rock fragmentation. *Rock. Mech. Rock. Eng.* **2024**, *57*, 3917–3935. [CrossRef]

Disclaimer/Publisher's Note: The statements, opinions and data contained in all publications are solely those of the individual author(s) and contributor(s) and not of MDPI and/or the editor(s). MDPI and/or the editor(s) disclaim responsibility for any injury to people or property resulting from any ideas, methods, instructions or products referred to in the content.